IIETA International Information and Engineering Technology Association
Advancing the World of Information and Engineering

Mathematical Modelling of Engineering Problems
Vol. 11, No. 8, August, 2024, pp. 2243-2250
Journal homepage: http://iieta.org/journals/mmep

Simulating the Tumor Mass Changes in PET and PET/CT Segmented Images Using Unsupervised Artificial Neural Network, HSOFM

Enam A. Salman, Rabab S. Abdoon, Loay E. George*

Department of Physics, College of Science, University of Babylon, Hilla 51001, Iraq

Corresponding Author Email: Loayedwar57@uoitc.edu.iq

https://doi.org/10.18280/mmep.110826

Received: 1 November 2023
Revised: 5 February 2024
Accepted: 25 February 2024
Available online: 28 August 2024

Keywords:
PET, PET/CT, FDG, Self-Organization Feature Map, image segmentation, neural networks, SUV, tumors

ABSTRACT

Image segmentation is one of the most important aspects of medical image processing. PET and PET/CT scanning are well-known imaging tools in medical image processing, which are used for figuring out the inner anatomy of the internal organs in a noninvasive manner. In this study, an unsupervised artificial neural network Hierarchical Self-Organizing Feature Map (HSOFM) is presented to isolate and extract abnormal regions in PET and PET/CT images. This method was implemented on three, images in which the tumor size decreases with time after receiving treatment, and then many mathematical models were tested to elect the proper one that more adequate to simulate the change behavior in order to predict the change in the tumor size in the coming time. The results indicate that this method was adequate to extract tumor areas with percentage the percent relative difference between the results of the proposed method and the radiologist work ranged from 0.00% to 33.766% for PET images and ranged from 5.809% to 34.459% for PET/CT scan images. The behavior of the abnormality size change with time was correctly simulated using exponential and linear mathematical models and the predicated tumor size values in the coming times were calculated the tumor size with over time for PET and PET/CT images. The resultant values of the coefficient of Determination (R^2) for the exponential model were 0.93, while for the linear model equation was 0.89. This is evidence of the success of the regression model in predicting future results.

1. INTRODUCTION

A non-invasive diagnostic technique that produces cross-sectional images and can be used to collect quantitative data regarding the metabolic activity of target tissues is called fluorine-18-fluorodeoxyglucose (^{18}F-FDG) positron emission tomography (PET). PET is widely utilized in tumor diagnosis and staging since its first in medicine. With the introduction of new radiotracers, PET has recently been employed in treatment planning and monitoring early response to therapy [1-3]. ^{18}F is a fluorine radioisotope created by cyclotrons that has a short half-life (109.7 min) and that emits positrons. It enables the tagging of a wide range of molecular tracers, which may be scanned within a few hours (usually) after. FDG is a glucose analogue that enters live cells via cell membrane glucose transporters and is then absorbed in the first phase of the regular glycolytic process. ^{18}F-labeled glucose analogue FDG is now utilized as a tracer. The amount of FDG accumulated in tissues is related to the amount of glucose used. Most malignant tumors have increased glucose uptake, overexpression of glucose transporters GLUT and increased hexokinase activity [1].

Fluorodeoxyglucose (^{18}F-FDG) is a popular tracer used in PET imaging to assess a patient's response to cancer diagnosis and therapy. Standard uptake values (SUVs) are then employed as a semi-quantitative strategy commonly utilized in tumor imaging. It is determined as the ratio of the radioactivity concentration in [kBq/ml] measured by a PET scanner inside the area of interest (ROI) to the quantity of FDG injected in [kBq] [4]. PET (^{18}F-FDG) has been used to assess therapy response in a variety of cancers. The findings suggested that ^{18}F-FDG positron emission tomography /Computed Tomography (PET/CT) might be used to identify responders from non-responders. Based on the retention of the radiotracer, ^{18}F-FDG positron emission tomography is a method capable of delivering metabolic information to cancer cells. This is due to the poor spatial resolution associated with this imaging technique, ^{18}F-FDG-PET scans have certain limitations in delivering reliable information on the outer and interior contours of the tumor. Although the most used tumor uptake value of 18F-FDG (SUV max) is widely used to reflect tumor lysis consumption on PET images, there is a tendency to use metabolic volume instead [5].

PET/CT is an imaging modality combining PET and (CT) scans to obtain information about metabolic activity in tissues and anatomical contexts. In PET-CT, beta- and gamma-radiation is used, i.e., ionizing radiation. Thus, its use must be well-motivated. In PET, metabolic activity is visualized by using a radiotracer that is beta radiation and is analogue to molecules participating in the process of interest. Thus, the

radiotracer accumulates in tissues with a high metabolic rate. The emitted positrons annihilate with a free electron within a few millimeters and emit two gamma rays in a direction opposite to each other. These photons are detected and the annihilation location can be reconstructed by sampling multiple events [6].

By detecting radiotracers, PET provides information about metabolic activity but not anatomy. Therefore, PET/CT scans have been introduced, combining PET scans with CT scans. Here, CT and PET scanners are set up next to each other and a patient first passes through them sequentially. The PET image can be mapped onto the CT image, providing anatomical information. The combined image has two image channels, i.e., one for the PET and one for the CT image [7, 8]. CT images are rebuilt and then sent to the PET workstation to give the attenuation correction factors needed for PET emission data reconstruction. Thus, PET and CT reconstructed images are merged and shown in the fusion workstation [8, 9]. the activity that is detected by the PET scanner is dependent on the injected dose as well as the weight of the patient, PET images are commonly normalized by using SUV. SUV measures the relative uptake of the radiotracer in the tissue. Its definition can be seen in Eq. (1) [8].

$$SUV = \frac{Tissue\ Activity\ [mCi/ml]}{Injected\ Dose\ [mCi/g]} \quad (1)$$

The first step in most image analysis procedures is segmentation, a process in which the image is divided into smaller parts. It generates multiple sets of pixels inside the same image. Every pixel in an image is assigned, and pixels with the same label share certain characteristics. Segmenting a digital image makes studying and recognizing key information easier [10]. The task determines the number of details with which the subdivision is carried out. In other words, segmentation should end after an application's objects or areas of interest have been discovered. Automated image segmentation aims to extract object boundary features and is fundamental to understanding image content [11, 12].

Many researchers have worked in this way, for example, Abdoon et. al. [13] proposed the HSOFM segmentation method and the results showed that the performance of HSOFM is promising compared to supervised neural networks. HSOFM technique was successful in correctly isolating and extracting the brain tumor. They concluded that the probability of extracting the tumor pixels with the largest possible size increases with increasing the number of clusters (increasing the main nodes). As the clusters increase, this area starts to decrease. This behavior is explained as follows: that is, as the number of clusters increases, the distribution of tumor pixels will be over more than one cluster (especially if it is known that the tumor area has a difference in density). They also concluded that the network with an increasing number of nodes needs to be properly trained to allow the network to extract as much information as possible by increasing the number of iterations.

Alwan [14] proposed methods to segment images CT- scan lungs that were classified as anomalies (COVID-19 and tumors) for the purpose of detecting, isolating, and extracting anomalous regions, using (an unsupervised, Hierarchical Self-Organizing Feature Map (HSOFM)) artificial neural networks. Clustering methods (K-Means and Fuzzy C-mean (FCM)) and a hybrid method are proposed to reduce the execution time required for HSOFM. These techniques were implemented using a number of clusters and a number of nodes (3, 4, 5). The results showed that the applied methods were sufficient for accurate detection and isolation. COVID-19 infected areas (95, 95, 94). (94%) for k-means, FCM, HSOFM, and hybrid Techniques, respectively, the results are consistent with the radiologist's identification of abnormal areas for COVID-19 and tumors.

In this study, the images of three successive scanning for abnormal case Hodgkin lymphoma, were adopted to segment them in order to extract the tumor region by implementing HSOFM unsupervised neural network. The behavior of the tumor size changes was simulated using two mathematical models to figure out the proper model and then adapt it to predicate the changes in the coming times.

2. SELF-ORGANIZATION FEATURE MAP ARTIFICIAL NEURAL NETWORK

The Self-Organization Feature Map (HSOFM) or SOM, proposed by Kohonen, is one of the more prominent artificial neural networks (ANN), The Self-Organizing Feature Map (HSOFM) or SOM was proposed by Kohonen. It is a feed-forward neural network developed used to segment medical images. SOFM is also known as the Kohonen map. It converts a high-dimensional space (n-dimensional input) to a low-dimensional space (two or one dimension). HSOFM is that provides a topology-preserving mapping from the input space to the clusters in a competitive network with self-organization, self-organizing maps utilize a neighborhood function to retain the topological qualities of the input space compared to other artificial neural networks. Let $X=(X_1\ X_2,\ldots X_p)'$ be the input vector (training case), and $W=(w_{l1}\ w_{l2},\ldots w_{lp})'$ be L is the weight vector associated with the node, w_{lj} indicates the weight assigned to input x_j to the node L, the number of nodes (cluster seeds) is L and the number of variables is P [15]. The self-organizing map is made up of components known as neurons or nodes. Of the same size as the input data vectors a weight vector and a position in the map space are associated with each node. The most common node configuration is a hexagonal or rectangular grid with consistent spacing. A higher-level input space to a lower-dimensional map space a self-organizing map represents. Finding the node with the closest weight vector to the vector obtained from data space and assigning the map coordinates of this node to our vector is the technique for inserting a vector from data space onto the map. The Euclidean distance between all weight vectors is calculated. The best matching unit (BMU) is the neuron with the most identical weight vector to the input. The weights of the BMU and neurons nearby in the SOM lattice are shifted in the direction of the input vector. The amount of the shift lessens over time and as one moves away from the BMU. The following is the updated formula for a neuron with a weight vector [16].

$Wv(i)$ is

$$\begin{aligned} Wv(i+1) &= Wi(i+1) \\ &= [wi(i) + hci(I)] * [(x(i) - w(i))] \end{aligned} \quad (2)$$

where, *hci* represents the neighborhood function to calculate it.

$$h(i) = \big(h(rc - r1)\big) * \big(a(i)\big) * alpha \quad (3)$$

where *rc*-*r*1 represents current neuron-next current neuron.

HSOFM maintains the most important topological and metric relationships for raw data elements. However, the primary application of HSOFM is dimensionality reduction, so it has been used for medical image segmentation [14]. numbers of nodes, six were adopted to segment the images under study by implementing the HSOFM method. Using this method, the procedure the following steps:

1. The input image is read.
2. Then HSOFM is performed with the number of nodes (6) on PET and PET/CT images.
3. After that, we determine the abnormal part.
4. Perform morphological operations, if necessary, such as opening with a structural element with a disc-shaped radius (5, 1, 1) for PET/CT images, respectively, this depends on the processed images.
5. Calculate the surface area of the extracted tumor regions.

3. THE CORRELATION COEFFICIENT (R)

The strength of the linear relationship between two variables, x and y, is referred to as the correlation coefficient. A positive relationship may appear with a linear correlation coefficient greater than zero. As for the negative relationship when the correlation coefficient has a value less than zero, there is no relationship between the variables x and y when the value of the correlation coefficient is zero [17].

4. COEFFICIENT OF DETERMINATION (R^2)

The coefficient of determination (R^2) is expressed in terms of the proportion of variation in the expected outcome. Its value ranges from 0 to 1 between the sample data and the expected data. The coefficient of determination indicates how well the regression model fits the data. That is, it represents the coefficient of determination calculated as the square of the correlation coefficient (R), The higher the value of the correlation coefficient, the closer the data estimated by the regression model of the resulting equation to the true data. The simple linear regression model is more successful in explaining the variance of y when the value of R^2 increases [18, 19]. Its number shows the percentage of variance that the regression equation can explain. A number of 1 indicates that each point on the regression line fits the data, and A value of 0.5 indicates that regression only explains half of the variance [17]. The coefficient of determination is widely used to demonstrate how well a regression model predicts future outcomes [17, 20]. The coefficient R^2 is commonly given as the percentage of variation explained by the response variable's (linear) relationship with the explanatory factors. It is calculated using the ratio [21].

$$R^2 = 1 - (A \,/\, M) \tag{4}$$

where, A represents sum of squared residue; M represents sum of squared total.

5. REGRESSION EQUATION

Regression is a technique for estimating the value of one of two variables using the value of the other. A regression equation is a mathematical expression of the relationship between two variables that can be used to estimate past values and forecast future values [17].

The multiple regression equation is written as

$$Y = f\,(\beta, X) + \varepsilon \tag{5}$$

where, X=X (X_1, X_2, ..., X_m) is the vector of independent variables; β is the vector of parameters (to be found); ε is the deviation; and Y is the dependent variable [22]. The relationship between two variables is measured by producing a straight-line equation of the simple linear regression model [17]

$$y = bx + a \tag{6}$$

There may be some variances of X in the forecast of the future value of Y. In general, the accuracy of this prediction is determined by the total number of predicted variables. Therefore, the larger the number, the more accurate the prediction. However, the regression equation is more complex. When a suitable computer programming language is not used, let alone done manually, this is why solving problems that require such an equation becomes very complicated; this leads to delays in the results [23].

Exponential regression model is a nonlinear regression model. The model parameters or variables are exponential and therefore the correlation between the variables is exponential [24].

$$y_i = a_0 + a_1\, e^{a_2 x} \tag{7}$$

where, y=[y_1, y_2, ..., y_n]^T the dependent variable x is the explanatory variable in the model, $a_0.a_1.a_2$. are the model parameter.

This is to prove the validation of exponential and linear mathematical models through the coefficient of determination (R^2) values.

6. SIMULATION OF CHANGE BEHAVIOR

Simulation is defined as a technique for studying dynamic systems in the real world whose behavior is imitated using a mathematical model of the system implemented on a digital computer. Computer simulation is a powerful methodology for the design and analysis of complex systems. To represent the dynamic properties of a system in the real world in a computer model is the comprehensive approach in computer simulation. Simulation is classified into discrete and continuous simulation. Continuous simulation, when the state variables change continuously with time, i.e., the set of variables required to describe the system, is called differential equations, and the behavior of the system is often described. Discrete simulation, when the state variables change at separate points in time, is called continual simulation [17].

7. THE MODELING OF CHANGES IN BEHAVIOR

After evaluating the changes and calculating the area of the tumor region in three successive scans of the patient, three mathematical models were adopted to investigate the proper one that simulate the area changes over time.

The calculated area (in pixels) and time (in month and day)

were plotted to introduce predictions about the changes for the time (one year) in the future. The following steps represent the change detection-modeling algorithm in a certain case:

Step 1: Using Microsoft Excel, assign the tumor area as the dependent variable and the image-year data as the independent variable.

Step 2: The data for these two variables should be drawn using a selecting curve.

Step 3: The coefficient of determination (R^2) represented the curve of each mathematical equation for the tumor area.

Step 4: To use the equation, the finest mathematical equation was chosen with the highest (R^2) to represent the tumor area as a dependent variable and the times of the categorized images as an independent variable.

8. MATERIALS AND METHODS

The working steps can be summarized block diagram in Figure 1.

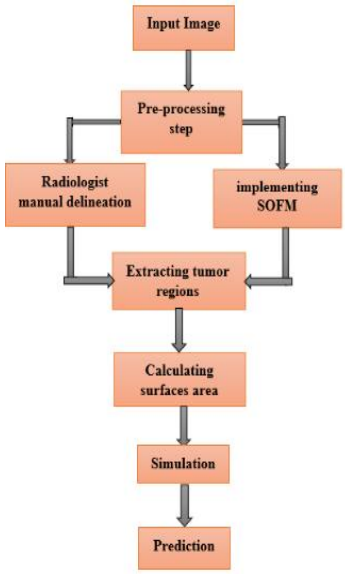

Figure 1. The block diagram of the procedure

The experimental images were acquired from Amir Al-Momineen Specialist Hospital in Iraq. The adopted images are for abnormal cases scanned at successive times for the purpose of studying the behavior of tumor change over time (with receiving the required treatment chemotherapy), as shown in Figure 2.

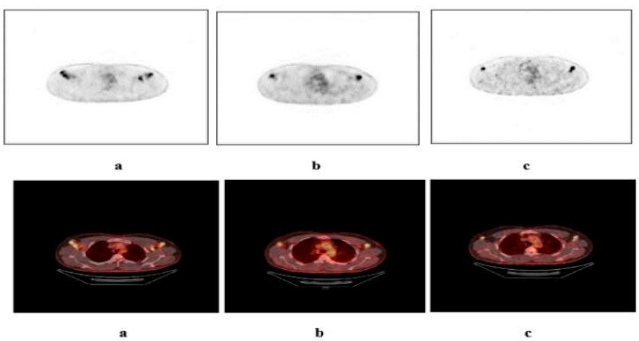

Figure 2. Experimental images the first row shows PET images, while the second row shows PET/CT images: (a) first scan (10) month, (b) second scan after (22.133) month and (c) third scan after (29.833) month

9. RESULTS AND DISCUSSION

9.1 Clustering HSOFM

The HSOFM technique was implemented on PET and PET/CT images by testing different numbers of nodes; the number six nodes were adopted because it gave the best extraction. Figures 3 and 4 present the results of segmenting the adopted images.

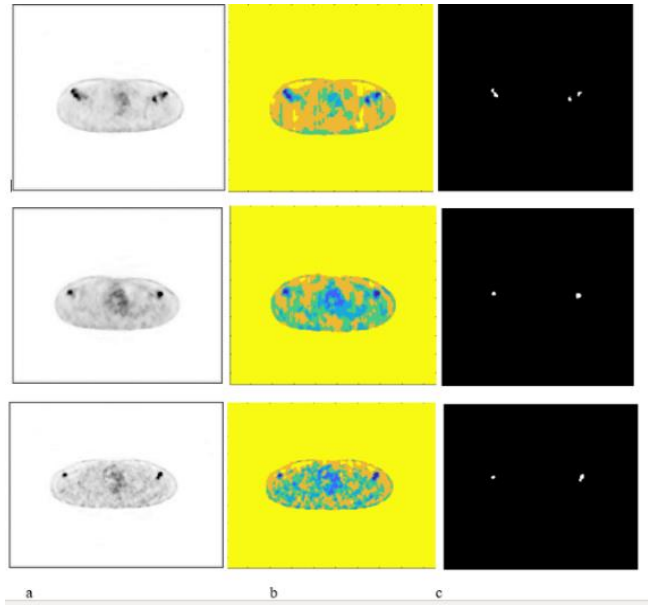

Figure 3. Results of implementing HSOFM on images PET with six nodes: (a) input images, (b) segmented images and (c) the final extracted tumor

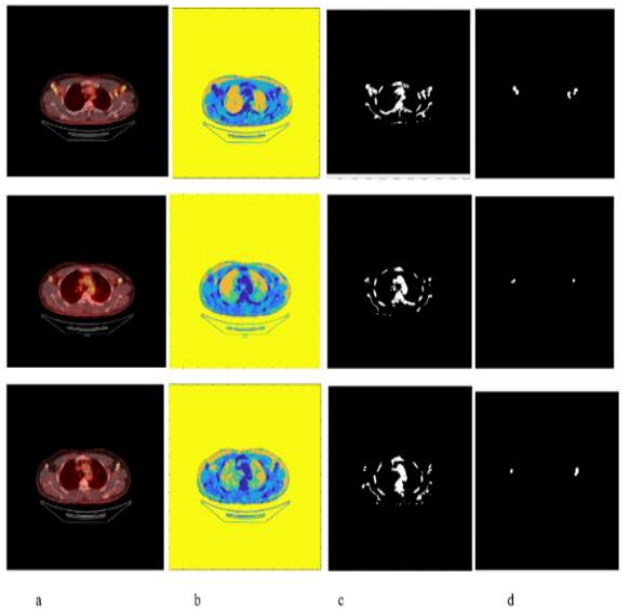

Figure 4. Results of implementing HSOFM on image PET/CT with six nodes: (a) input images; (b) segmented images; (c) the cluster of the infected region; (d) the final extracted tumor

Figures 3 and 4 also show the results of implementing the HSOFM algorithm with a number of nodes (6) for PET and PET/CT images, The results showed an adequate extraction of the infected regions according to the radiologist consultation.

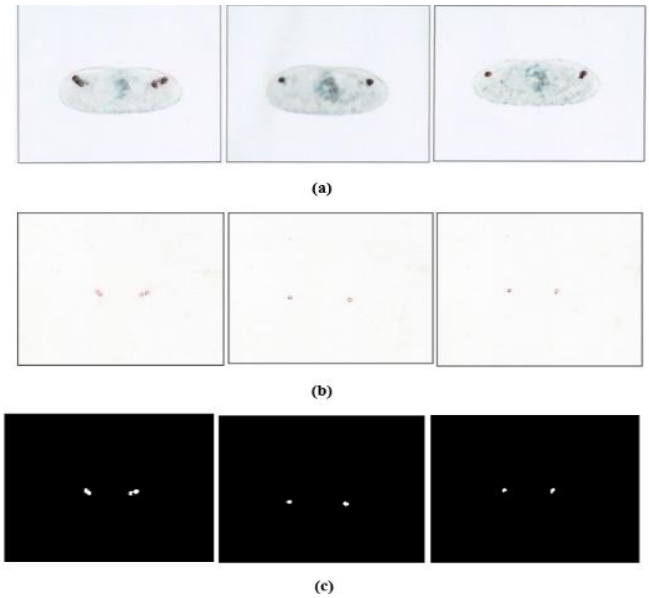

Figure 5. Radiologist manual delineation of abnormal area for PET images

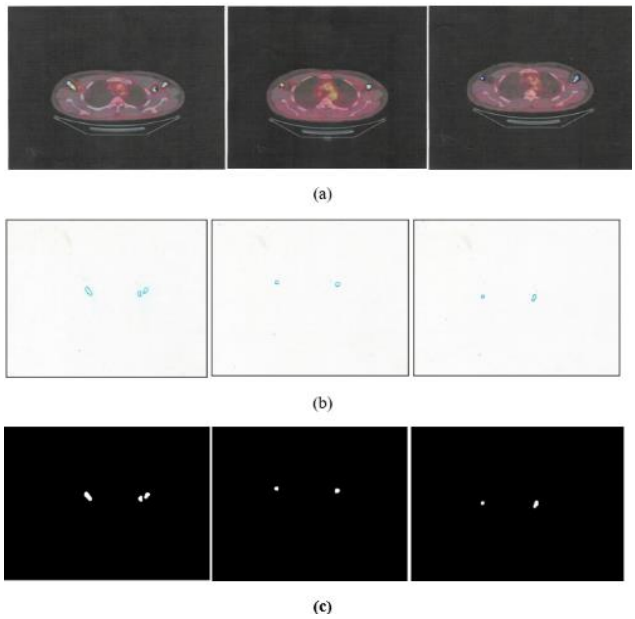

Figure 6. Radiologist manual delineation of abnormal area for PET/CT images

9.2 Radiologist delineation

The experimental PET images and PET/CT images, for radiologist were introduced for manual delineation of the abnormal regions. After processing the selected images to extract the outline boundaries of the abnormal areas. Using suitable image processing functions to fill the contouring regions, these objects, representing abnormal regions (tumors), were extracted and the surface area of these regains, were calculated to use them as ground truth to investigate the performance quality of the implemented segmenting method.

Figures 5 and 6 show the results of these steps for PET scan and PET/CT images, respectively, (a) shows the abnormal regions by radiologist delineation, (b) represents the delineation contour only, while (c) indicates the filled delineation of the abnormal areas when part of the image processing functions is applied.

9.3 Simulation steps

More than one mathematical model was tried to figure out the more adequate one that simulates the behavior of the change in tumor size over time. The available models include the linear model, second-degree polynomial model, logarithmic model, and the exponential model. The most common simulations were the linear and exponential models, the results of which are presented in Figures 7 and 8. They present the simulation of the tumor size (in blue) for exponential and linear, respectively.

The coefficient of determination R^2 describes the relationship between the area of tumors in pixels and the times in months. In addition to that, it determines the extent to which the region of the variable of the tumor depends on the independent variable times, of where A: (tumors area) t: (month).

When plotting the relationship between the area of the tumor as a dependent variable and the general value of the images, which were classified as an independent variable, the study that tumor area tended to decrease at different rates.

During the study, the highest value of the coefficient of determination (R^2) for exponential model for PET /CT images was (R^2=0.93%), followed by exponential model for PET images was (R^2=0.91%), followed by linear model for PET images was (R^2=0.89), and linear model for PET /CT images was (R^2=0.81%), indicating that the best equation; exponential model for followed by linear model.

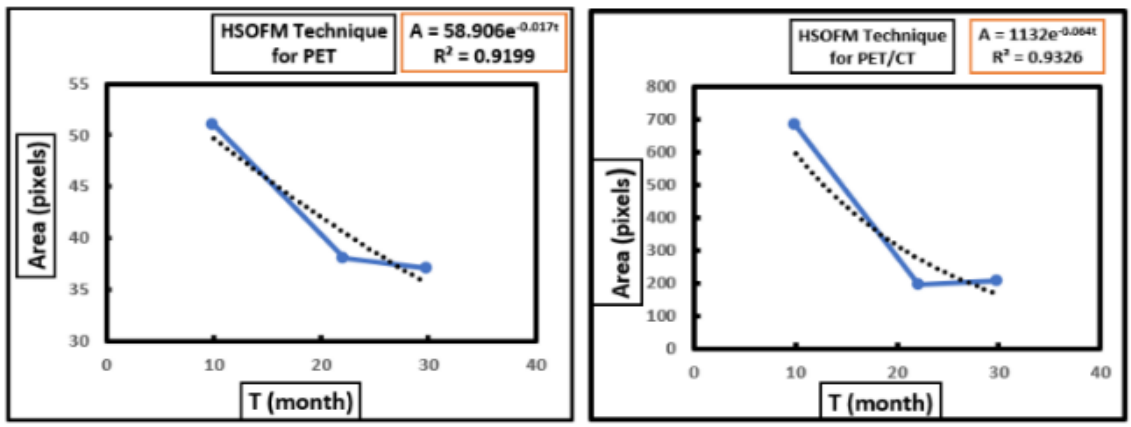

Figure 7. Simulate the behavior of the change in tumor size over time by adopting an exponential model: (a) for PET images and (b) for PET/CT images

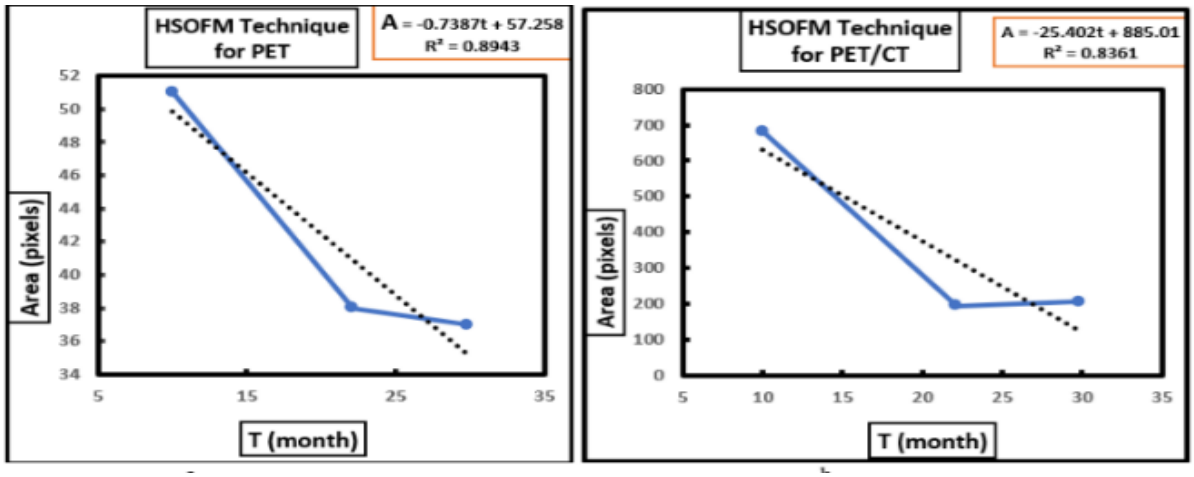

Figure 8. Simulate the behavior of the change in tumor size over time by adopting a linear model: (a) for PET images and (b) for PET/CT images

9.4 Prediction step

In this step, the two proposed mathematical models (exponential and linear) were adopted to calculate the tumor size in many coming times and the prediction of the tumor size (in brown), for exponential and linear, respectively. The results of which are presented in Figures 9 and 10.

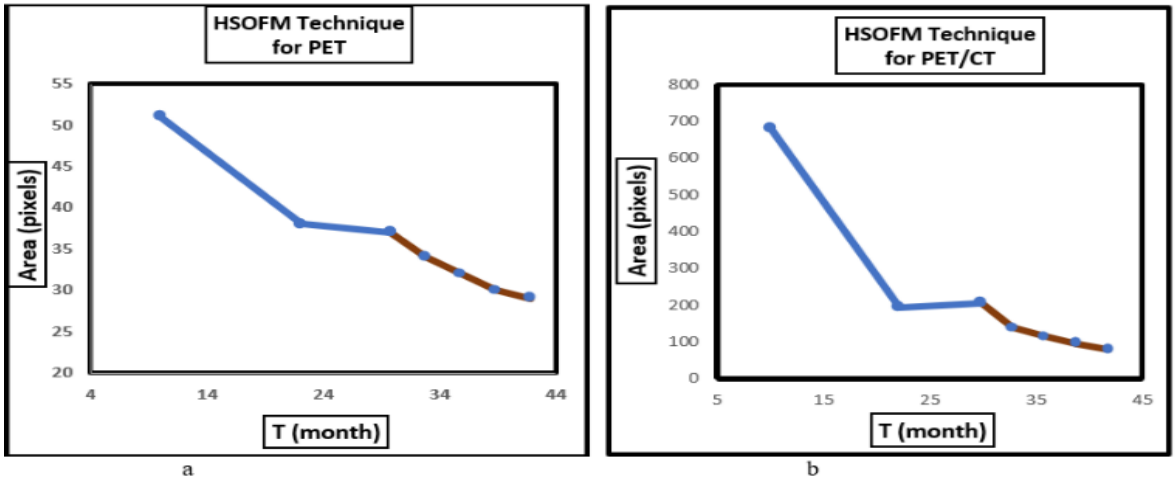

Figure 9. Combining simulates the behavior of the change in tumor size and the prediction of the tumor size over time by adopting an exponential model: (a) PET images and (b) PET/CT images

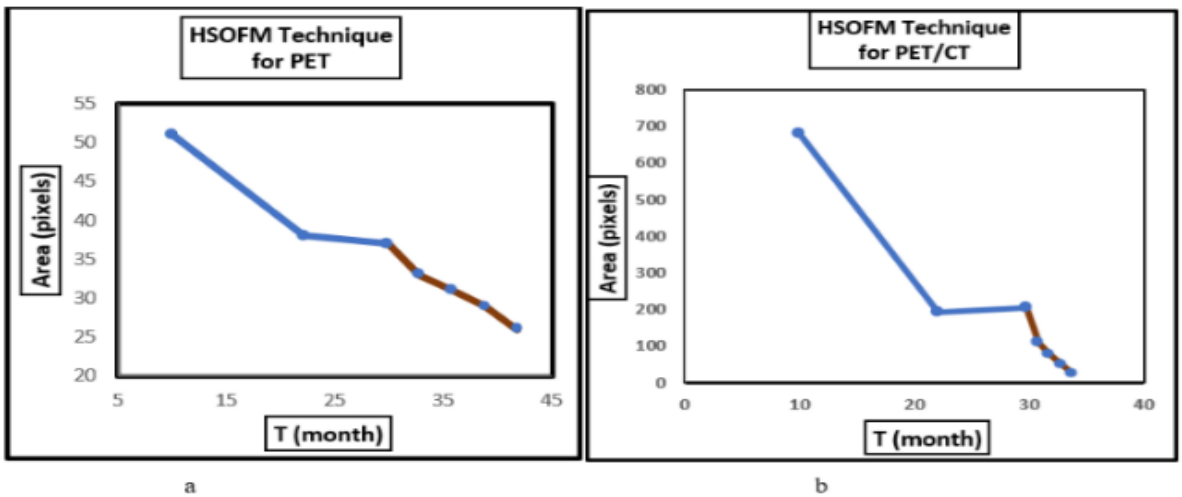

Figure 10. Combining simulates the behavior of the change in tumor size and the prediction of the tumor size over time by adopting a linear model: (a) PET images and (b) PET/CT images

9.5 Calculating surface area

A. In this step, the calculated extracted surface area of the affected area and the radiologist's specialist's demarcation area of the PET and PET/CT images were calculated the percent relative presented in Table 1.

Table 1. The time calculated values with surface area calculated for extracted tumor area and nuclear medicine specialist demarcation area

Image No.	Time (Months)	PET			PET/CT		
		Surface Area (Pixels)	Area of Radiologist (Pixels)	Relative Difference of Area %	Surface Area (Pixels)	Area of Radiologist (Pixels)	Relative Difference of Area %
Image1	10	51	77	33.766	681	723	5.809
Image2	22.133	38	42	9.523	194	296	34.459
Image3	29.833	37	37	0	206	275	25.090

By close inspection of Tabel 1, one can conclude that there is a proper number of nodes that is adequate for clustering each image under study depending on the intensity variance of the objects within each of them. The percent relative difference between the results of the proposed method and the radiologist work ranged from 0.00% to 33.766% for PET images and ranged from 5.809% to 34.459% for PET/CT scan images.

B. In this step, the calculated extracted surface area is the prediction of the tumor size over time for PET and PET/CT images using the two proposed mathematical models (exponential and linear) and presented in Tables 2 and 3.

Table 2. Surface areas calculated tumor prediction over time for PET images

Image No.	Time (Months)	Exponential Model	Linear Model
		Expected Surface Area (Pixels)	Expected Surface Area (Pixels)
Image1	32.833	34	33
Image2	35.833	32	31
Image3	38.833	30	29
Image4	41.833	29	26

Table 3. Surface areas calculated tumor prediction over time for PET/CT images

Image No.	Exponential Model		Linear Model	
	Time (Months)	Expected Surface Area (Pixels)	Time (Months)	Expected Surface Area (Pixels)
Image1	32.833	138	30.833	108
Image2	35.833	114	31.833	76
Image3	38.833	94	32.833	51
Image4	41.833	78	33.833	26

10. CONCLUSIONS

In this work, HSOFM was employed for extracting abnormal regions in PET and PET/CT scanning images three successive times. The results indicate that this method was adequate to extract tumor areas with a percentage difference ranging between from 0.00% to 33.766% for PET images and ranged from 5.809% to 34.459% for PET/CT scan images the radiologist delineation. The behavior of the size change with time was correctly simulated using exponential and linear mathematical models, and the predicated tumor size values in the coming times were calculated. the finding of the equation for each tumor through mathematical modeling, the resultant values of the coefficient R^2=0.91-0.93 for the exponential model were, while for the linear model, equation was R^2=0.81-0.83. The simulation step used the equations generated through the mathematical modeling for each class to predict the area of the tumor. The simulation results showed the future state of each tumor area up to the one year, the tumor decreased because he received chemotherapy.

ACKNOWLEDGMENT

The authors would like to thank Radiologist Dr. Karrar Obaid Al-Mansoori, Head of Nuclear Medicine Department at Amal Al-Hayat Hospital for Cancer and Blood Diseases, for his identification of the tumor areas and his consultation and review when extracting the tumor using the depended technique. The authors would also like to thank Amir Al-Momineen Specialized Hospital for providing the PET and PET/CT images.

REFERENCES

[1] Boellaard, R., Delgado-Bolton, R., Oyen, W.J., Giammarile, F., Tatsch, K., Eschner, W., Verzijlbergen, F.J., Barrington, S.F., Pike, L.C., Weber, W.A., Stroobants, S., Delbeke, D., Donohoe, K.J., Holbrook, S., Graham, M.M., Testanera, G., Hoekstra, O.S., Zijlstra, J., Visser, E., Hoekstra, C.J., Pruim, J., Willemsen, A., Arends, B., Kotzerke, J., Bockisch, A., Beyer, T., Chiti, A., Krause, B.J. (2015). FDG PET/CT: EANM procedure guidelines for tumour imaging: Version 2.0. European Journal of Nuclear Medicine and Molecular Imaging, 42: 328-354. https://doi.org/10.1007/s00259-014-2961-x

[2] Tamal, M. (2020). Intensity threshold based solid tumour segmentation method for Positron Emission

Tomography (PET) images: A review. Heliyon, 6(10): e05267. https://doi.org/10.1016/j.heliyon.2020.e05267
[3] Moussallem, M., Valette, P.J., Traverse-Glehen, A., Houzard, C., Jegou, C., Giammarile, F. (2012). New strategy for automatic tumor segmentation by adaptive thresholding on PET/CT images. Journal of Applied Clinical Medical Physics, 13(5): 236-251. https://doi.org/10.1120/jacmp. v13i5.3875
[4] Baazaoui, A., Barhoumi, W., Zagrouba, E., Mabrouk, R. (2016). A survey of PET image segmentation: Applications in oncology, cardiology and neurology. Current Medical Imaging, 12(1): 13-27.
[5] Fagundes, T.C., Mafra, A., Silva, R.G., Castro, A.C., Silva, L.C., Aguiar, P.T., Silva, J.A., Junior, E.P., Machado, A.M., Mamede, M. (2018). Individualized threshold for tumor segmentation in 18 F-FDG PET/CT imaging: The key for response evaluation of neoadjuvant chemoradiation therapy in patients with rectal cancer? Revista da Associação Médica Brasileira, 64: 119-126. https://doi.org/10.1590/1806-9282.64.02.119
[6] Tong, S., Alessio, A.M., Kinahan, P.E. (2010). Image reconstruction for PET/CT scanners: Past achievements and future challenges. Imaging in Medicine, 2(5): 529-545. https://doi.org/10.2217/iim.10.49
[7] Erondu, O.F. (2011). Medical imaging. Intech Open.
[8] Stahnke, L. (2023). TransRUnet: 2D Detection and Segmentation of Lymphoma Lesions in Full-Body PET-CT Images. Kth Royal Institute of Technology.
[9] Vasilou, A.K. (2021). Clinical implementation of PET/CT imaging in radiotherapy treatment planning. M.Sc. Thesis. University of Patras.
[10] Balber, T., Tran, L., Benčurová, K., Raitanen, J., Egger, G., Mitterhauser, M. (2022). Experimental nuclear medicine meets tumor biology. Pharmaceuticals, 15(2): 227. https://doi.org/10.3390/ph15020227
[11] Schöder, H., Erdi, Y.E., Larson, S.M., Yeung, H.W. (2003). PET/CT: A new imaging technology in nuclear medicine. European Journal of Nuclear Medicine and Molecular Imaging, 30: 1419-1437. https://doi.org/10.1007/s00259-003-1299-6
[12] Chan, T., Zhu, W. (2005). Level set based shape prior segmentation. In 2005 IEEE Computer Society Conference on Computer Vision and Pattern Recognition (CVPR'05), Diego, USA, pp. 1164-1170. https://doi.org/10.1109/CVPR.2005.212
[13] Abdoon, R.S., Abood, L.K., Ali, S.M. (2015). Detection of brain tumor in MRI utilizing supervised neural networks and adaptive HSOFM algorithm. IOSR Journal of Applied Physics (IOSR-JAP), 7(3): 26-41. https://doi.org/10.9790/4861-07332641
[14] Alwan, A.A.H. (2023). Utilizing multi-image processing techniques to detect and isolate abnormalities in medical images. M.Sc. Thesis, University of Babylon, Iraq.
[15] Abdoon, R.S. (2014). Adaptive techniques for brain tumor detection. Ph.D. Thesis, University of Baghdad, Iraq.
[16] Logeswari, T., Karnan, M. (2010). An improved implementation of brain tumor detection using segmentation based on soft computing. Journal of Cancer Research and Experimental Oncology, 2(1): 6-14.
[17] Wdaah, I.R. (2022). Using multispectral satellite images for the sustainable development of Karbala governorate. M.Sc. Thesis. University of Kufa.
[18] Campos, W.V., Teixeira Filho, J., São José, A.R. (2023). Regression equation for correlation between Spad index and photosynthetic pigments under saline stress in African mahogany culture. International Journal of Science and Research Archive, 8(2): 647-655. https://doi.org/10.30574/ijsra.2023.8.2.0314
[19] Muhsi, M., Suprapto, S., Rofiuddin, R. (2023). The node selection method for split attribute in C4. 5 algorithm using the coefficient of determination values for multivariate data set. Jurnal Penelitian Pendidikan IPA, 9(7): 5574-5583. https://doi.org/10.30574/ijsra.2023.8.2.0314
[20] Nagelkerke, N.J. (1991). A note on a general definition of the coefficient of determination. Biometrika, 78(3): 691-692.
[21] Renaud, O., Victoria-Feser, M.P. (2010). A robust coefficient of determination for regression. Journal of Statistical Planning and Inference, 140(7): 1852-1862. https://doi.org/10.1016/j.jspi.2010.01.008
[22] Aliyev, Q.S, Hajiyeva, R.J., Ahmadova, E.N., Asgerova, B.H., Almammadova, M.H., Alesker, İ.A. (2023). Construction of multiple regression equations for studying regularities of chemical processes. Journal of Pharmaceutical Negative Results, 14(2): 1066-1072. https://doi.org/10.47750/pnr.2023.14.02.137
[23] Anichebe, G.E. (2022). Programming multi-linear regression equation for faster problem-solving and decision-making. Anchor University Journal of Science and Technology, 2(2): 134-142.
[24] Irshayyid, A.J., Saleh, R.A. (2023). Robust estimates for a three-parameter exponential regression model. International Journal of Nonlinear Analysis and Applications, 14(1): 2799-2808. https://doi.org/10.22075/ijnaa.2023.29395.4148